Tracing low temperature fluid flow on ridge-flanks with sedimentary uranium distribution

Mills, R.A.[1] and Dunk, R.M.[1,2]

1 National Oceanography Centre, Southampton, University of Southampton, Southampton, SO14 3ZH, UK.

2 Present address: Crichton Carbon Centre, Rutherford McCowan Crichton University Campus, Dumfries, DG1 4ZH, UK.

Corresponding author email: Rachel.Mills@soton.ac.uk, Tel: +44 (0)23 80592678, Fax: +44 (0)23 80593052

Abstract

Low-temperature, ridge-flank hydrothermal reaction is an important component of heat and chemical exchange. The uranium content of sediments and pore fluids along a ridge-axis to ridge-flank transect perpendicular to the southern East-Pacific Rise is described. Two distinct regions are identified: (1) the ridge-crest (0.36 Ma crust) where significant solid phase U enrichments occur and (2) the ridge-flank (1.9-4.6 Ma crust) with constant

U association with hydrothermal Fe oxide phases in the solid phases and no ongoing in situ reaction of pore fluids with sediments. Upward advection and diffusion of cool, U-depleted basement fluids occurs at many coring sites. At the ridge-crest site the oxic basal fluids strip the plume derived sediment of the excess U, effectively migrating the U upwards through the sediment into the overlying water column. At the ridge-flank sites the pore fluid advection rates are highest at bathymetric/basement highs and advection velocities of up to 7.5 mm yr^{-1} are inferred from the pore fluid profiles. These estimates are consistent with previous calculations based on fluoride pore fluid distributions. The basal fluid U depletions are in the range 10-70% depending on temperature and redox state and thus low-temperature uptake of U during basalt alteration is a significant sink from seawater. Pore fluid U content is a sensitive tracer of extremely low temperature (<5^{o}C) and low velocity (<10 mm yr^{-1}) advection through ridge-flank systems and the basal sediment U/Fe ratio is potentially a useful proxy for basement alteration history.

240 words

Key Words: uranium, low-temperature hydrothermalism, east pacific rise

Geochemical cycles 0330

Sedimentary geochemistry 1051

Hydrothermal systems 3017

40

41 1. Introduction

42 The magnitude and locus of hydrothermal circulation remains poorly constrained in
43 ocean biogeochemical budgets. In particular, a large geochemical exchange flux may be
44 associated with low-temperature fluid flow through mid-ocean ridges and overlying
45 sediments leading to significant chemical exchange with seawater [*Maris and Bender*,
46 1982; *Nielsen et al.*, 2006]. This low-temperature exchange at temperatures only
47 marginally above seawater values is extensive in areas of thin sediment cover or
48 topographic highs that penetrate thicker sediment [*Fisher et al*., 2003; *Wheat and*
49 *McManus*, 2008].

50 Uranium is removed from seawater during high-temperature hydrothermal exchange
51 [*Michard and Albarede*, 1985] and significant depletion is also seen in low-temperature
52 fluids (62-64^{o}C; [*Wheat et al.*, 2002]) and thus may provide a useful tracer of lower
53 temperature hydrothermal fluid flow. The U content of basalt alteration products in areas
54 of low-temperature hydrothermalism also implies that significant uptake of U occurs
55 during basaltic reaction with circulating seawater [*Dunk et al.*, 2002; *Bach et al.*, 2003;
56 *Schramm et al.*, 2005]. However, relatively little is known about the behaviour and
57 geochemical cycling of U in pore fluids and sediments during low-temperature
58 hydrothermalism in ridge-crest and flank sediments where significant fluid fluxes are
59 inferred to occur with temperature anomalies of 0.1-3.6^{o}C relative to seawater [*Nielsen et*
60 *al*., 2006]..

Ridge-crest metalliferous hydrothermal sediments contain significant levels of a range of trace metals, with typical U contents in near-vent field sediments of ~10 ppm [*Veeh and Boström*, 1971; *Rydell et al.*, 1974; *Mills et al.*, 1994; *Schaller et al.*, 2000]. Hydrothermal plume particles scavenge U from the water column via co-precipitation with Fe (hydr)oxides, and have a U/Fe ratio (wt/wt) of ~1.8×10^{-6} [*German et al.*, 1991]. Sedimentary U/Fe ratios (~20×10^{-6}) are significantly higher than those reported for oxide plume particulates [*German et al.*, 1991]. The reported $^{234}U/^{238}U$ activity ratio [*Bender et al.*, 1971; *Veeh and Boström*, 1971; *Mills et al.*, 1994] of the authigenic component of hydrothermal sediments is within analytical error of the seawater value (1.144; [*Chen et al.*, 1986]), indicating a seawater source for this element.

Sulfidic hydrothermal plume particles can have U/Fe ratios two orders of magnitude higher than oxide dominated systems and the source of U is also inferred to be seawater [*German et al.*, 2002]. Uranium rich sulfides (dominantly FeS_2) may be transported to ridge-crest sediments where the fate of the sulfide material depends on the redox status of the sediment and rate of burial [*Mills et al.,* in review]. In near-field hydrothermal mound deposits on the Mid-Atlantic Ridge (MAR) and rise crest sediments on the East Pacific Rise (EPR), observed U/Fe ratios are not constant but show a high degree of variation, ranging from ~20×10^{-6} to > 400×10^{-6} [*Mills et al.*, 1994; *Schaller et al.*, 2000; *Mills et al.*, in review]. Conversely, older sediments (e.g. fully oxidised mound debris on the MAR or far field ridge-flank sediments on the EPR), whilst maintaining a high U/Fe ratio with respect to oxide plume particulates, display a relatively constant, low U/Fe ratio on the order of 20×10^{-6}, suggesting that at least part of the observed U enrichment is a transitory feature [e.g. *Mills et al.*, 1994].

We present new data from the active eastern flank (0-5 Ma) of the EPR at 14-15^{o}S where low-temperature fluid flow is largely controlled by basement topography [*Grevemeyer et al.*, 2002; *Villinger et al.*, 2002]. We sampled the basement fluids by full penetration of the sediment column [c.f. *Wheat and McManus*, 2008] and demonstrate that oxic fluid flow has a significant impact on the preservation of uranium peaks in the sediment. We demonstrate the successful use of pore fluid U distribution as a tracer of fluid flow in this region of extremely low-temperature, high water-rock ratio flow and propose that basal sediment U/Fe ratios may be used as a proxy for extensive, oxic, low-temperature alteration of the underlying basement..

2. Sampling and Methods

The EXCO study area is a 720km long and 40-90km wide region east of the ridge axis which intersects the ridge axis of the SEPR at 14°14'S, 60km to the south of the Garrett transform fault and north of a minor ridge discontinuity at 14°27'S (Fig. 1). During the EXCO II/2 cruise (January-February 2000) a suite of sediment cores were collected by gravity corer (with a 6m core barrel) from 3 regions overlying oceanic crust with palaeomagnetic ages of 0.36, 1.9 and 4.6Ma (Fig. 1; Table 1). Cores were collected at each site to reflect variations in local bathymetry and heat flow. Cores 12, 17, 19, 20, 24 and 28 sampled basement (i.e. the core catcher was severely dented and basalt was recovered) and thus basement fluid composition can be inferred from the deepest pore fluid compositions [*Wheat and McManus*, 2008] (Table 1).

Pore fluids were separated by centrifugation of 2-5cm sections of undisturbed sediment core (8-15 samples per core, 30-50 cm depth intervals). All samples were handled at

106 temperatures <4ºC during centrifugation and filtration of the supernatant through
107 Whatman 0.45 μm filters into acid cleaned, polypropylene vials. Sediment samples were
108 taken from the same depth horizon. Sampling artefacts arising from oxic handling of
109 these sediment cores are inferred to be minimal at the low Fe and Mn concentrations
110 observed [*Wheat and McManus*, 2008]. Eight cores (4 from the 0.36Ma site (core 12, 17,
111 18 and 19), 3 from the 1.9Ma site (core 10, 20 and 24) and 1 from the 4.6Ma site (core
112 7)) were selected for bulk sediment digests and a more detailed sequential extraction
113 procedure was also employed on one core (core 12).

114 0.2 g of dried, ground sediment were digested via a 4 stage procedure; (1) an aqua regia
115 attack (2.5ml), where the samples were refluxed at 90ºC overnight and dried down at
116 100ºC; (2) a combined hydrofluoric and perchloric acid attack (HF, 2 ml; $HClO_4$, 1.5 ml),
117 where the samples were refluxed at 150ºC overnight and dried down at 170ºC, increasing
118 to 190ºC on the observation of white fumes; (3) an $HClO_4$ attack (2 ml), where the
119 samples were immediately dried down at 190ºC; (4) dissolution in hydrochloric acid (6M
120 HCl, 10ml), where the samples were placed in a thermostatically controlled oven at 60ºC
121 overnight.

122 The sequential extraction scheme described by *Bayon et al.* [2002] was used to separate
123 the sediment (core 12) into four operationally defined fractions: (1) carbonate-bound and
124 adsorbed or readily exchangeable species removed using 10% acetic acid (CAE); (2) acid
125 reducible 'amorphous' Mn and Fe (hydr)oxides removed using 1M hydroxylamine/25%
126 acetic acid (AM); (3) organic material removed using 5% hydrogen peroxide (ORG); and

(4) residual material including crystalline iron oxides assessed by complete digestion of the residual phase (RES).

All ICP-AES analyses (Fe, Mn, P, V, Ca, Ti, Al.) were performed on a Perkin Elmer Optima 4300DV instrument. Standards were matrix matched and the RSD of replicate analysis of unknowns was generally better than 2% for all elements presented here. All ICP-MS analyses for U concentration were carried out on a quadrapole mass spectrometer (VG PlasmaQuad 2+ instrument) fitted with an electron multiplier detector. A peak-jumping analytical mode was employed where ion counts were measured at m/z^{+} ratios of 235, 236 and 238. 0.5 g of porewater were diluted to a final mass of 5g using 2% (v/v) SBD HNO_3 spiked with a known amount of ^{236}U. Analytical uncertainty for porewater analyses is estimated to be 10% based on analysis of Pacific seawater. 6 replicate digests and analyses of the USGS MAG-1 standard gave a full method precision of 2.9% RSD for solid phase U analysis.

2.1 Pore fluid modelling

Pore fluid advection velocities can be estimated in short cores (<10m) which are at steady state using the standard one dimensional diagenetic advection-diffusion-reaction equation by assuming that reaction is negligible and that there are no significant changes in porosity or tortuosity with depth [*Maris and Bender*, 1982]. If we assume that the uppermost measured $[U]_{pw} = C_0$ and that the deepest $[U]_{pw}=C_{base}$ then the solution to the advection-diffusion equation is:

$$C_z = C_0 + A\left(\exp\left(\frac{v.z}{D_s}\right) - 1\right)$$

$$A = \frac{C_{base} - C_0}{\exp\left(\frac{v.z_{base}}{D_s}\right) - 1} \qquad \text{Equation 1}$$

Where v is the advective pore fluid velocity, D_s is the whole sediment diffusion coefficient for U and z is depth below seafloor. The whole sediment diffusion coefficient was calculated from the diffusion coefficient at infinite dilution (D^0) for temperature and tortuosity. Given the small measured temperature gradient in these cores [*Villinger et al.*, 2002], the sediment temperature (T) was assumed to be constant and equal to the average mid-depth temperature at the ridge-flank 1.9Ma (2.9°C) and 4.6Ma (2.6°C) sites. The diffusivity of U at $T_{mid\text{-}depth}$ was estimated from the diffusivity at 25°C (4.26 x 10^{-6} cm^2 s^{-1}; [*Li and Gregory*, 1974] and the Stokes-Einstein diffusion coefficient temperature dependence relationship [*Li and Gregory*, 1974] scaled for the estimated temperature (T):

$$\frac{D^0_{25^oC}}{D^0_{0^oC}} = 2.19 \qquad \text{Equation 2}$$

Sediment tortuosity (θ) is estimated from the measured average sediment porosity (ϕ; 0.72 at the 1.9Ma site and 0.64 at the 4.6Ma site) [*Boudreau*, 1997]

$$\theta^2 = 1 - \ln\left(\phi^2\right) \qquad \text{Equation 3}$$

and this is used to correct D^0 at the *in situ* temperature (T):

$$D_{S,T} = \frac{D^0_T}{\theta^2} \qquad \text{Equation 4}$$

163 $D_{S,T}$ for the 1.9Ma site is 1.33 x 10^{-6} cm^2 s^{-1} and 1.15 x 10^{-6} cm^2 s^{-1} for the 4.6Ma site.

164 The pore fluid advection velocity (v) was estimated by fitting an advection –diffusion
165 profile to the observed measurement and the best-fit solution was obtained by minimizing
166 the sum of the squares of the residual concentration difference between the observed and
167 estimated $[U]_{pw}$. No advection-diffusion-reaction modelling was carried out for the pore
168 water profiles indicating significant reaction as the reactions for U are poorly constrained
169 and subject to sampling artefacts.

170 2.2 Geological setting and pore fluid characterisation

171 The full spreading rate at the superfast spreading SEPR at 14°14'S is 143-150 mm yr^{-1}
172 [*Grevemeyer et al.*, 2002]. The ridge-crest site at 0.36Ma crust is characterised by
173 smooth terrain and thin sediment cover [*Villinger et al.*, 2002]. Heat flow measurements
174 are significantly below the crustal cooling model predictions confirming that
175 hydrothermal advection of seawater through the thin sediment cover has cooled the
176 basement to temperatures close to that of bottom water (2-3°C; [*Villinger et al.*, 2002].
177 Both the ridge-crest (0.36Ma) site and the young ridge-flank (1.9Ma) site have lines of
178 abyssal hills which form a series of ridges that run parallel to the strike of the ridge-crest
179 (013º). The 4.6Ma site is between two medium to large sized seamounts [*Villinger et al.*,
180 2002]. The sediment cover is thin (<3m) on the steep flanks of the northern seamount
181 and increases to >20m between the two seamounts [*Villinger et al.*, 2002]. High heat-
182 flow values measured at the base of the seamount suggest that there is low-temperature
183 discharge in this region. Basalt alteration along the EXCO transect is consistent with

184 low-temperature oxic to suboxic reactions with measurable uptake of U, Ca and K during
185 alteration [*Schramm et al.*, 2005].

186 Previous modelling of pore fluid profiles of nitrate and fluoride suggest that there is slow
187 (~mm yr^{-1}) advective flow through the sediment at ridge-crest and ridge-flank sites at
188 basement highs [*Mottl and Wheat*, 2000]. Advection-diffusion-reaction modelling of Si
189 data from the 0.36Ma site demonstrate that basalt derived formation fluids are seeping
190 through the thin sediment cover at rates of 10-200 mm yr^{-1} [*Wheat and McManus*, 2008].
191 The formation fluids in the permeable upper oceanic crust are low-temperature, largely
192 oxic and 'leak' to the overlying seawater where basement approaches the seafloor or
193 other permeability constraints allow fluid advection [*Villinger et al.*, 2002]. The oxic
194 formation fluids at the 0.36 ridge-crest site have Mg contents indistinguishable from
195 seawater with some loss of Si to secondary minerals during basement reaction [*Mottl and*
196 *Wheat*, 2000; *Wheat and McManus*, 2008]. Reaction with basement and loss of nitrate
197 and fluoride in the formation fluid is seen at the 1.9Ma site [*Mottl and Wheat*, 2000]. The
198 chlorinity of all formation fluids was within 0.7% of modern seawater implying that the
199 age of the basement fluids is <2000 years at all sites [*Mottl and Wheat*, 2000].

200 3. Results

201 All solid phase sediment data have been corrected for salt content by subtraction of the
202 pore fluid salts estimated from porosity and chlorinity measurements; this correction is
203 negligible for the data presented here (Table 2; Supplementary Tables 1a-c). The
204 carbonate content was estimated from the detrital corrected Ca data and the hydrothermal
205 component by difference (Hydrothermal = Total – carbonate – detrital); [*Dunk and Mills*,

206 2006]. The carbonate content of EXCO sediments varies from 65-95% [*Dunk and Mills*,
207 2006] and the hydrothermal component within the sediment is significant (30-34%) at
208 140-165cmbsf for the ridge-crest samples but relatively minor through most of the ridge-
209 flank sediments (<12%). The hydrothermal rich horizon at mid-depth is apparent in all of
210 the ridge-crest cores (Fig. 4) implying a general enrichment in hydrothermal input to this
211 site at this time.

212 Uranium in the EXCO sediments displays a different behaviour in the ridge-crest and
213 ridge-flank environments with clear excess U present at the ridge-crest sites (Fig. 2). In
214 the ridge-crest region (the 0.36Ma site), the U content of the sediment reaches values of
215 8-13 ppm in the upper layers of each core sampled and displays a wide range in U/Fe_{ex}
216 (up to ~380 x 10^{-6}). In the ridge-flank environment (the 1.9 and 4.6Ma study sites), the U
217 content of the sediment is low, ranging from 0.2 to 1.4 ppm, and the U/Fe ratio is
218 relatively constant (~30 x10^{-6}). At the ridge-crest site (0.36Ma) the sequential leach data
219 allow partitioning of the U and Fe into 4 operationally defined fractions (Fig. 3; Table 2).

220 The pore water data for near surface sediments (0-10 cmbsf) consistently display U
221 contents $[U]_{pw}$ lower than seawater values ([U] = 13.9±0.9 nM). There are difficulties
222 associated with the collection of porewater samples for U analysis because of well
223 documented sampling artefacts, most likely due to depressurisation during core collection
224 and precipitation of carbonate which tends to lead to artificially low $[U]_{pw}$ values
225 compared with the seawater value of ~13.9 nM [*Toole et al.*, 1984]. The carbonate
226 alkalinity, Mg and Ca content of EXCO pore fluids was determined onboard during
227 EXCOII/2 and measurements were close to seawater values at all sites [*Mottl and Wheat*,

228 2000] indicating that no significant perturbations to the carbonate chemistry are occurring
229 during sampling. Near surface $[U]_{pw}$ values are as high as 12.7nM at the 4.6Ma site but
230 much lower (6-9nM) at other sites. We attribute the non-seawater upper core $[U]_{pw}$
231 values to significant (1m+) loss of surface sediment with the 6m barrel gravity coring
232 technique used which often recovered nearly 6m of sediment on hitting basement. This is
233 consistent with other tracer measurements (e.g. Fluoride which show significant surface
234 depletions relative to seawater [*Mottl and Wheat*, 2000].

235 The observed variation in $[U]_{PW}$ greatly exceeds the estimated analytical uncertainty of
236 10%, and the maximum $[U]_{PW}$ varied from 9.6 to 29.1 nM. The rapid desorption or
237 oxidation (with subsequent release to the fluid phase) of sedimentary U is a known
238 potential sampling artefact (e.g. [*Anderson et al.*, 1989]). High $[U]_{PW}$ at depth in sediment
239 cores has also been attributed to the transfer of U bearing sediment particles across a 0.45
240 μm filter. If either of these artefacts were the cause of the high $[U]_{PW}$ observed in this
241 study, then the greatest effect would be expected in the deeper samples with the highest
242 U_{bulk} and U_{CAE} in the solid phase. This is not observed and therefore we infer that this
243 artefact is not important at this site.

244 The pore fluid data from the ridge-crest site show the largest range in $[U]_{pw}$ content. The
245 same general profile is seen in the majority of the ridge-crest cores with a minimum at
246 20-50cmbsf and a mid-depth maxima at ~150 cmbsf or deeper (Fig. 4). The ridge-flank
247 sites (1.9Ma and 4.6Ma) all show depletion of $[U]_{pw}$ relative to the overlying seawater
248 with significant curvature indicative of upward advection and diffusion of a depleted
249 basal fluid at several sites.

The U content of basal pore fluids in ridge-crest cores 12 and 19 situated along the bathymetric high show good agreement at 10.9±0.3 nM and 10.8±0.4 nM respectively. The deeper core 17 basal fluid is closer to seawater composition (15 nM). At the 1.9Ma site two different basal pore fluid compositions were sampled. At the Western site the basal pore fluids are oxic (measurable nitrate, $[U]_{pw}$=8.3-8.6 nM). At the Eastern site which is situated on a basement high [*Grevemeyer et al.*, 2002] the basal pore fluids are suboxic (zero nitrate, measurable Mn, [*Mottl and Wheat*, 2000] and the $[U]_{pw}$ for the basal fluid is 4.3 nM. The basal fluid $[U]_{pw}$ at the oxic 4.6Ma site at the base of a seamount is 11.3-11.7 nM. Downcore pore fluid $[U]_{pw}$ profiles for the ridge-flanks sites are compared with model values in Fig. 5 and estimated upward advective velocities are shown in Table 1. There is broad agreement between estimates of upwelling velocity using $[U]_{pw}$ distribution and that estimated from fluoride data [*Mottl and Wheat*, 2000].

4. Discussion

In the ridge-flank region (1.9 and 4.6Ma crust), U shows a constant linear relationship to Fe, with U/Fe ratios comparable to previously reported values for oxic metalliferous sediments [*Mills et al.*, 1994]. A least squares fit through the U-Fe ridge-flank data gives a U/Fe (wt/wt) ratio of 32×10^{-6}. The uniformity of the U/Fe ratio across all samples from the 1.9 and 4.6Ma sites in addition to the basal samples from the 0.36Ma sites suggests a constant association between U and Fe in oxic metalliferous sediments exposed to basal fluid flow. This phase association of U and Fe is assessed through the sequential leach analysis of ridge-crest core 12 which has elevated U/Fe ratios in the upper core and oxic U/Fe ratios near basement (Fig. 3; Table 2).

In core 12, the majority of U was extracted in the CAE fraction (ca. 70-80%; Fig. 3; Table 2). The carbonate material in the EXCO sediments is dominated by calcite (foraminifera and coccoliths). The CAE fraction represents loosely bound or adsorbed U, although given the propensity of U(VI) to form soluble carbonate complexes (e.g. $UO_2(CO_3)_2^{2-}$ and $UO_2(CO_3)_3^{4-}$) in concentrated carbonate solutions, this fraction may also include soluble U(VI) compounds. Approximately 80-90% of the bulk sediment U in the basal 0.36Ma sample was associated with the CAE fraction (Fig. 3a), implying that the U is dominantly adsorbed to the Fe (hydr)oxide surface as opposed to incorporated into the crystalline structure. This fraction of U, once fixed through adsorption, is assumed to be permanently associated with the Fe, where the $(U/Fe)_{oxic}$ ratio represents saturation of surface adsorption sites for U. The similarity in the down core U distribution in each operationally defined leach (Fig. 3a) suggests a pervasive enrichment of U throughout the core, rather than a specific mineralogical association. The excess U inventory (U_{bulk} – $Fe_{hydrothermal}$*$(U/Fe)_{oxic}$) is assumed to be labile during oxic diagenesis and subject to further diagenetic reaction, ultimately leading to loss from the sediment column and a whole core profile displaying a constant, oxic U/Fe ratio.

Heat-flow measurements at the ridge-crest indicates that hydrothermal advection of heat occurs at this site cooling the crust [*Villinger et al.*, 2002]. Pore fluid nitrate profiles indicate an oxic basement fluid at all sites and fluoride profiles indicate no advection at core 12 but significant upward flow (6 mm yr^{-1}) at the core 18 site atop an abyssal hill (~3200 m water depth) [*Mottl and Wheat*, 2000]. The $[U]_{pw}$ data indicate that significant

293 reaction occurs within the sediment column at all ridge-crest sites and no simple
294 advection-diffusive fit is possible for the data (Fig. 4).

295 The general decrease observed from the surface sample $[U]_{PW}$ to a local minimum at
296 relatively shallow depths at the ridge-crest site indicates that *in situ* reaction and uptake
297 of $[U]_{pw}$ is occurring in the uppermost part of the core. The solid phase maxima and
298 U/Fe_{ex} maxima coincide with this pore fluid minima (Fig. 4) supporting this inference.
299 The ridge-crest cores are fully oxic throughout (nitrate = seawater values [*Mottl and*
300 *Wheat*, 2000], therefore a reductive mechanism [e.g. *Morford et al.*, 2009] of removal is
301 ruled out. Given the high affinity of U for co-precipitation with Fe (hydr)oxides [e.g.
302 *Duff et al.*, 2002], this diffusive flux may be driven by adsorption and complexation of U
303 during oxic alteration of ferrihydrite, rather than a reductive process.

304 Pore water data for the 0.36Ma site shows a broad $[U]_{pw}$ peak at the same depth as the
305 solid phase hydrothermal peak (Fig. 4). This is attributed to *in situ* oxidation of any U-
306 rich sulphides to ferrihydrite and alteration of amorphous to more crystalline Fe-oxides
307 which is inferred to release U into pore fluids. Under suboxic conditions this $[U]_{pw}$ will
308 coprecipitate with oxide phases and carbonates [*Mills et al.*, in review] but in an area of
309 active fluid flow supplying oxidants to the base of the sediment column the $[U]_{pw}$ will be
310 remobilised and lost from the sediment over time. At the 0.36Ma site, the basal pore
311 fluids are oxic with near seawater nitrate concentration and zero Mn in solution [*Mottl*
312 *and Wheat*, 2000]. Upwards advection of pore fluids is apparent in the fluoride data from
313 core 18 (5.8 mm yr^{-1}; Table 1) and widespread seepage of basaltic formation fluids has
314 been inferred from pore water Si profiles [*Wheat and McManus*, 2008]. The upwards
315 migration of the solid phase U is controlled by a mechanism analogous to the burn-down

316 of oxygen and relocation of sedimentary U in turbiditic sediments [*Colley and Thomson*,
317 1985], but where the source of the mobilising fluid is from basement rather than the
318 sediment-water interface. The net effect of the upward diffusion (and advection) of
319 oxygenated fluids is to strip the lower sediments of the excess U inventory (Fig. 4).

320 Subseafloor U enrichments in SEPR metalliferous sediments along the EPR [*Rydell et al.*,
321 1974; *Schaller et al.*, 2002] have recently been attributed to enhancement in sulphide (and
322 therefore U) supply to the sediment during Pleistocene glacials under lower bottom water
323 oxygen conditions [*Mills et al.*, in review]. The primary U enrichment is retained in the
324 sediment during alteration of sulphide to ferrihydrite to crystalline Fe oxides as long as
325 oxidation occurs below the surface mixed layer and no significant oxidation of the deeper
326 sediment occurs during ridge-flank low-temperature fluid flow. On the thinly sedimented
327 eastern flank of the EPR the significant fluid flow relocates the plume derived U from the
328 sediment to the overlying water column.

329 Pore fluid advection velocity (v) can only be determined where basal fluids have a
330 measurable contrast with overlying seawater values (Fig. 5). Advection of basal fluids
331 depleted in U is apparent at a number of ridge-flank sites associated with bathymetric
332 highs and pore fluid advection rates up to 7.5 mm yr^{-1} are estimated using the $[U]_{pw}$
333 distribution. $[U]_{pw}$ appears to be a good tracer of low-temperature (<5^{o}C) and low
334 velocity (<10 mm yr^{-1}) fluid advection in the ridge-flank setting. Fluoride has also been
335 shown to be a useful tracer of pore fluid advection in low-temperature systems [*Maris et*
336 *al.*, 1984] and there is close agreement in the calculated advection velocity estimated
337 from $[F]_{pw}$ and $[U]_{pw}$ data for cores 10, 23 and 24 from the 1.9Ma Eastern ridge-crest site
338 (Table 1) supporting the validity of the estimates from the $[U]_{pw}$ data. This is in contrast

339 with nutrient profiles which are unreliable at low fluid advection rates [*Wheat and*
340 *McDuff*, 1995]. Mg and Ca data at all sites are very close to seawater values minimizing
341 the utility of these classic tracers in this setting.

342 The concentration of U in basal pore fluids indicates that basement fluids can become
343 significantly depleted in U (ca. 10-70%), even at very low alteration temperatures (<5ºC).
344 The extent of U depletion estimated at both the 0.36 and 4.6Ma sites, where basement
345 fluids are oxic with a temperature of ca. 3.0-3.4ºC [*Villinger et al.*, 2002], is comparable,
346 with an estimated depletion of 10-20% relative to seawater. At the 1.9Ma site, where
347 fluids are slightly warmer (4.0ºC; [*Villinger et al.*, 2002], the extent of U depletion is
348 comparatively higher, with an estimated removal of 35-40% in oxic fluids, and 65-70% in
349 reducing fluids.

350 Low-temperature alteration processes in the ridge-flank setting are a function of crustal
351 permeability and sediment cover. The small amount of U uptake in EXCO basalts is
352 inferred to be associated with celadonite formation in the upper crust under oxic
353 conditions [*Schramm et al.*, 2005]. The observed uptake of U is low relative to other
354 estimates [*Hart and Staudigel*, 1982; *Kelley et al.*, 2003]. The lowest basal U content for
355 EXCO formation fluids is 4.3 nM which implies that U uptake from circulating seawater
356 is up to 70% effective at the low-temperatures observed on the EXCO ridge-flank despite
357 the evidence for minimal solid phase uptake of U.
358
359
360 5. Conclusions

Ridge-crest sediments at 15°S on the SEPR display elevated U/Fe ratios typical of MOR near-field sediments which are inferred to be derived from U rich sulphide particles transported by plume dispersal. Basal ridge-crest and ridge-flank sediment have lower near constant U/Fe ratios similar to oxic hydrothermal sediments from other ridge settings (U/Fe = 32 x 10^{-6} wt/wt). In this high fluid-flow environment, oxidation of the ridge-crest sediment column occurs via diffusion and advection of basal fluids through the sediment pile which strips the sediment of excess U which is associated with primary sulphidic hydrothermal inputs and their alteration products. Thus any palaeorecord of past U/Fe distribution is lost from the sediment in areas of active oxic fluid flow. The U/Fe ratio of basal sediments is a potential proxy for low-temperature oxic formation fluids and could be useful in mapping out the distribution of such fluids.

The fitting of a one dimension advection-diffusion model to the pore-water U data confirms that fluids are upwelling along an abyssal hill ridge-crest at the 1.9Ma site and on the steep flanks of the seamount at the 4.6Ma site at rates of up to 7.5 mm yr^{-1}. The removal of U to ocean crust at temperatures close to ambient seawater is an important sink from seawater. These data suggest that pore water U and sedimentary U/Fe ratios could be valuable tracers of both low temperature and low velocity fluid flow in regions away from ridge-crest reaction.

Acknowledgements: We are indebted to Colin Devey, Mike Mottl, Geoff Wheat and the shipboard complement aboard the R/V Sonne during cruise SO-145/2. Darryl Green and

382 Andy Milton provided invaluable laboratory support at NOCS. This work was supported
383 by NERC through grant GR3/11984 and studentship GT/04/99/ES/256.

384

385 References

386

387 Anderson, R. F., M. Q. Fleisher, and A. P. Lehuray, Concentration, oxidation-state, and
388 particulate flux of uranium in the Black-Sea, *Geochimica et Cosmochimica Acta*, 53,
389 2215-2224, 1989.
390 Bach, W., B. Peucker-Ehrenbrink, S. R. Hart, and J. S. Blusztajn, Geochemistry of
391 hydrothermally altered oceanic crust: DSDP/ODP Hole 504B - Implications for seawater-
392 crust exchange budgets and Sr- and Pb-isotopic evolution of the mantle, *Geochemistry*
393 *Geophysics Geosystems*, 4, 2003.
394 Bayon, G., C. R. German, R. M. Boella, J. A. Milton, R. N. Taylor, and R. W. Nesbitt,
395 An improved method for extracting marine sediment fractions and its application to Sr
396 and Nd isotopic analysis, *Chemical Geology*, 187, 179-199, 2002.
397 Bender, M., W. Broecker, V. Gornitz, U. Middel, R. Kay, S.-S. Sun, and P. Biscaye,
398 Geochemistry of three cores from the East Pacific Rise, *Earth and Planetary Science*
399 *Letters*, 12, 425-433, 1971.
400 Boudreau, B. P., *Diagenetic models and their implementation: modelling, transport and*
401 *reaction in aquatic sediments*, 414 pp., Springer, Berlin, 1997.
402 Chen, J. H., R. L. Edwards, and G. J. Wasserburg, U-238,U-234 and Th-232 in seawater,
403 *Earth and Planetary Science Letters*, 80, 241-251, 1986.

404 Colley, S., and J. Thomson, Recurrent uranium relocations in distal turbidites emplaced
405 in pelagic conditions, *Geochimica et Cosmochimica Acta*, 49, 2339-2348, 1985.
406 Duff, M. C., J. U. Coughlin, and D. B. Hunter, Uranium co-precipitation with iron oxide
407 minerals, *Geochimica et Cosmochimica Acta*, 66, 3533-3547, 2002.
408 Dunk, R. M., and R. A. Mills, The impact of oxic alteration on plume-derived transition
409 metals in ridge flank sediments from the East Pacific Rise, *Marine Geology*, 229, 133-
410 157, 2006.
411 Dunk, R. M., R. A. Mills, and W. J. Jenkins, A reevaluation of the oceanic uranium
412 budget for the Holocene, *Chemical Geology*, 190, 45-67, 2002.
413 Fisher, A. T., E. E. Davis, M. Hutnak, V. Spiess, L. Zuhlsdorff, A. Cherkaoui, L.
414 Christiansen, K. Edwards, R. Macdonald, H. Villinger, M.J. Mottl, C.G. Wheat and K.
415 Becker, Hydrothermal recharge and discharge across 50 km guided by seamounts on a
416 young ridge flank, *Nature,* 421, 618-621, 2003.
417 German, C. R., A. P. Fleer, M. P. Bacon, and J. M. Edmond, Hydrothermal scavenging at
418 the Mid-Atlantic Ridge - radionuclide distributions, *Earth and Planetary Science Letters*,
419 105, 170-181, 1991.
420 German, C. R., S. Colley, M. R. Palmer, A. Khripounoff, and G. P. Klinkhammer,
421 Hydrothermal plume-particle fluxes at 13 degrees N on the East Pacific Rise, *Deep-Sea*
422 *Research Part I-Oceanographic Research Papers*, 49, 1921-1940, 2002.
423 Grevemeyer, I., B. Schramm, C. W. Devey, D. S. Wilson, B. Jochum, J. Hauschild, K.
424 Aric, H. W. Villinger, and W. Weigel, A multibeam-sonar, magnetic and geochemical
425 tow-line survey at 14^{o}14'S on the southern East Pacific Rise - insights into the fourth

426 dimension of ridge crest segmentation, *Earth and Planetary Science Letters*, 199, 359-
427 372, 2002.
428 Hart, S. R., and H. Staudigel, The control of alkalis and uranium in sea-water by ocean
429 crust alteration, *Earth and Planetary Science Letters*, 58, 202-212, 1982.
430 Kelley, K. A., T. Plank, J. Ludden, and H. Staudigel, Composition of altered oceanic
431 crust at ODP Sites 801 and 1149, *Geochemistry Geophysics Geosystems*, 4, 2003.
432 Li, Y. H., and S. Gregory, Diffusion of ions in sea-water and in deep-sea sediments,
433 *Geochimica et Cosmochimica Acta*, 38, 703-714, 1974.
434 Maris, C. R. P., and M. L. Bender, Upwelling of hydrothermal solutions through ridge
435 flank sediments shown by pore water profiles, *Science*, 216, 623-626, 1982.
436 Maris, C. R. P., M. L. Bender, P. N. Froelich, R. Barnes, and N. A. Luedtke, Chemical
437 evidence for advection of hydrothermal solutions in the sediments of the Galapagos
438 Mounds hydrothermal field, *Geochimica et Cosmochimica Acta*, 48, 2331-2346, 1984.
439 Michard, A., and F. Albarede, Hydrothermal uranium uptake at ridge crests, *Nature*, 317,
440 244-246, 1985.
441 Mills, R. A., S. L. Taylor, P. H. Pälike, and J. Thomson, Hydrothermal sediments record
442 changes in deep water oxygen content in the SE Pacific, *Paleoceanography*, in review,
443 2010.
444 Mills, R. A., J. Thomson, H. Elderfield, R. W. Hinton, and E. Hyslop, Uranium
445 enrichment in metalliferous sediments from the Mid-Atlantic Ridge, *Earth and Planetary*
446 *Science Letters*, 124, 35-47, 1994.

447 Morford, J. L., W. R. Martin, and C. M. Carney, Uranium diagenesis in sediments
448 underlying bottom waters with high oxygen content, *Geochimica et Cosmochimica Acta*,
449 *73,* 2920-2937, 2009.
450 Mottl, M. J., and C. G. Wheat, Hydrothermal fluxes on mid-ocean ridge flanks: EXCOII
451 on the eastern flank of the East Pacific Rise near 14^{o}S., American Geophysical Union
452 Fall Meeting, San Francisco, 2000.
453 Nielsen, S. G., M. Rehkamper, D. A. H. Teagle, D. A. Butterfield, J. C. Alt and A. N.
454 Halliday, Hydrothermal fluid fluxes calculated from the isotopic mass balance of thallium
455 in the ocean crust, *Earth and Planetary Science Letters*, 251, 120-133, 2006.
456 Rydell, H., T. Kraemer, K. Bostrom, and O. Joensuu, Postdepositional injections of
457 uranium-rich solutions into East Pacific Rise sediments, *Marine Geology*, 17, 151-164,
458 1974.
459 Schaller, T., J. Morford, S. R. Emerson, and R. A. Feely, Oxyanions in metalliferous
460 sediments: Tracers for paleoseawater metal concentrations?, *Geochimica et*
461 *Cosmochimica Acta*, 64, 2243-2254, 2000.
462 Schramm, B., C. W. Devey, K. M. Gillis, and K. Lackschewitz, Quantitative assessment
463 of chemical and mineralogical changes due to progressive low-temperature alteration of
464 East Pacific Rise basalts from 0 to 9 Ma, *Chemical Geology*, 218, 281-313, 2005.
465 Toole, J., J. Thomson, T. R. S. Wilson, and M. S. Baxter, A Sampling Artifact Affecting
466 the Uranium Content of Deep-Sea Porewaters Obtained from Cores, *Nature*, 308, 263-
467 266, 1984.
468 Veeh, H., and K. Boström, Anomalous $^{234}U/^{238}U$ on the East Pacific Rise, *Earth and*
469 *Planetary Science Letters*, 10, 372-374, 1971.

Villinger, H., I. Grevemeyer, N. Kaul, J. Hauschild, and M. Pfender, Hydrothermal heat flux through aged oceanic crust: where does the heat escape?, *Earth and Planetary Science Letters*, 202, 159-170, 2002.

Wheat, C. G., and R. E. McDuff, Mapping the fluid-flow of the Mariana Mounds ridge flank hydrothermal system - pore-water chemical tracers, *Journal of Geophysical Research-Solid Earth*, 100, 8115-8131, 1995.

Wheat, C. G., and J. McManus, Germanium in mid-ocean ridge flank hydrothermal fluids, *Geochemistry Geophysics Geosystems*, 9, Q03025, doi:10.1029/2007GC001892, 2008.

Wheat, C. G., M. J. Mottl, and M. Rudnicki, Trace element and REE composition of a low-temperature ridge-flank hydrothermal spring, *Geochimica et Cosmochimica Acta*, 66, 3693-3705, 2002.

Figure Captions

Figure 1: Map showing coring locations for this study. The EXCO region is shown and three regions of interest are highlighted. Insets show coring locations within each area.

Figure 2: Inter-element plot for U and Fe in EXCO cores. Crosses are ridge-crest samples (0.36Ma), open circles are ridge-flank samples (1.9Ma) and open triangles are ridge-flank samples (4.6Ma). The dashed line indicates the U/Fe ratio for fully oxic metalliferous sediments [*Mills et al*., 1994].

Figure 3: Sequential leach data for ridge-crest hydrothermal sediments (core 12). Down-core plot of (a) Fe partitioning into operationally defined phases from the sequential leach

492 data (method adapted from [*Bayon et al.*, 2002]: Dark grey shading (CAE) = carbonate
493 associated and exchangeable Fe, light grey shading (AM) = amorphous Fe oxides and
494 mid grey shading (RES) = residual crystalline Fe. Red line indicates total bulk analysis.
495 and (b) U sequential leach data (shading as for (a)).

496 Figure 4: Down-core plots of the estimated hydrothermal component (grey shading), pore
497 fluid U content (crosses) and U/Fe solid phase ratio (hatched area) for ridge-crest sites (a)
498 core 12, (b) core 19, (c) core 17 and (d) core 18. Arrows indicate bottom water
499 composition at the EXCO site; seawater values are approached at the core top and near
500 basement.

501 Figure 5: Down-core pore fluid U content for the ridge-flank 1.9Ma (West and East) and
502 the 4.6Ma sites which show upward advective flow. 1.9Ma West: open squares = core
503 20, closed triangles = core 21, 1.9Ma East: open circles = core 24, closed circles = core
504 10, crosses = core 23, 4.6 Ma: closed triangles = core 7, open circles = core 4, crosses =
505 core 25, closed circles = core 26, open squares = core 27. Dashed lines show the
506 advection-diffusion model fits through each data set (see text).

507

508

509

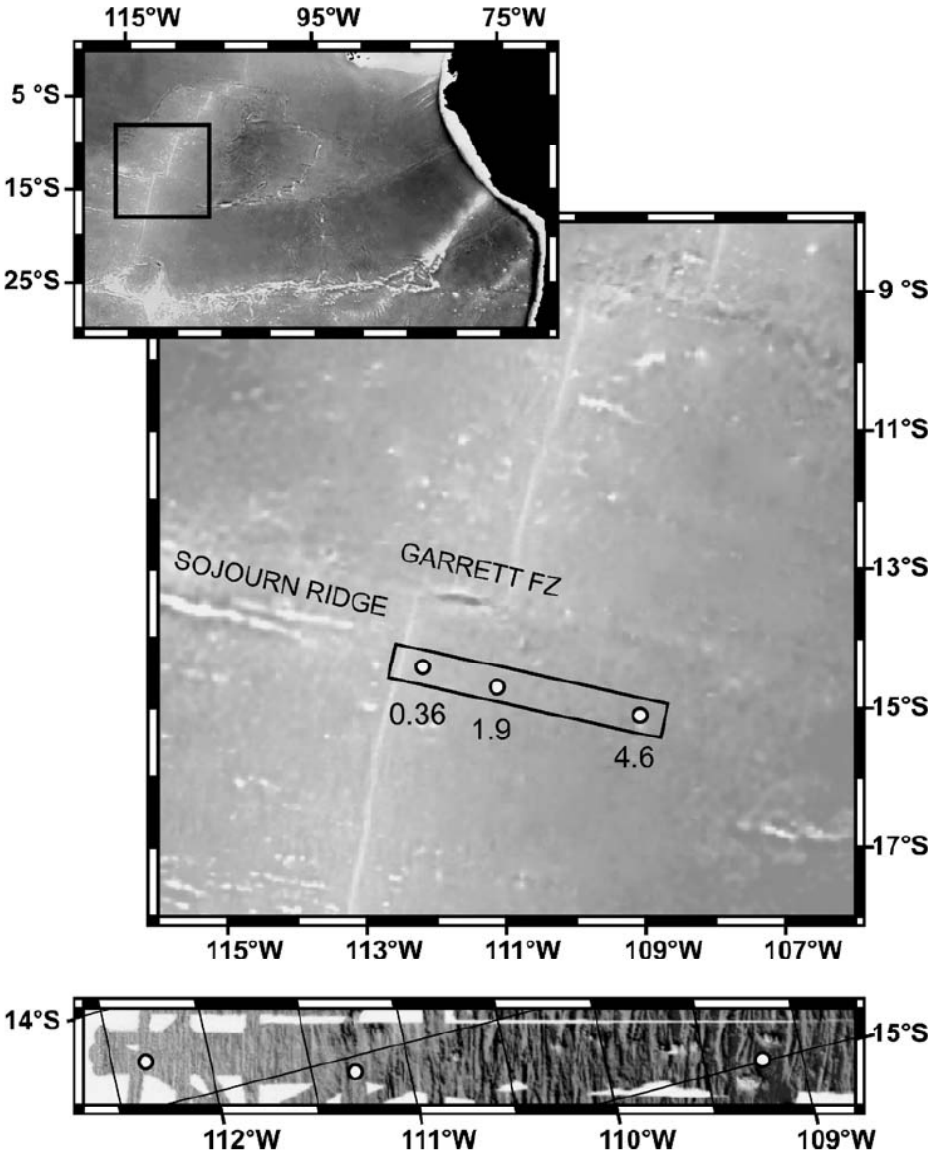

Dunk and Mills, Figure 1

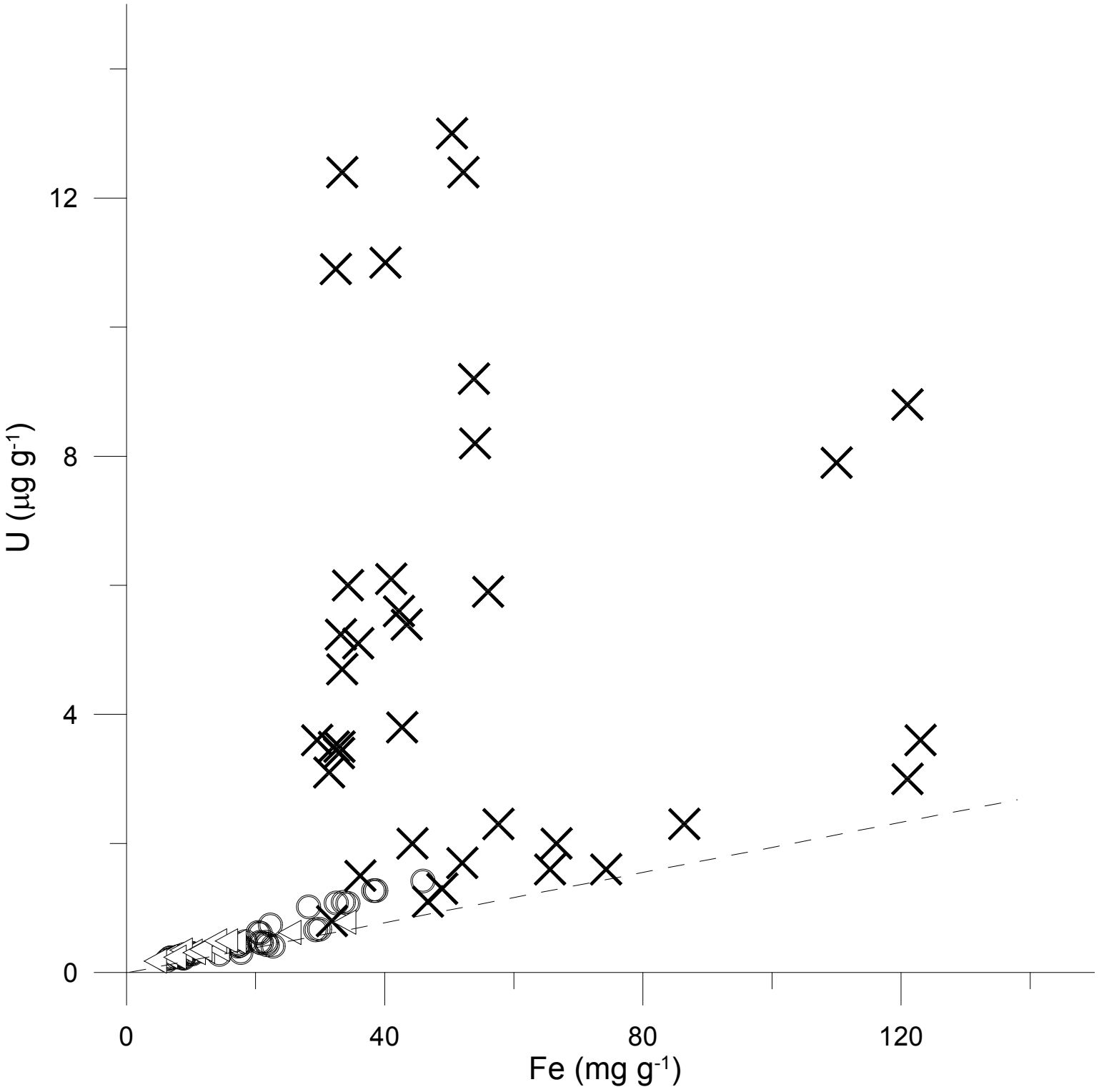
12
8
4
0
U (µg g-1)
0
40
80
120
Fe (mg g-1)

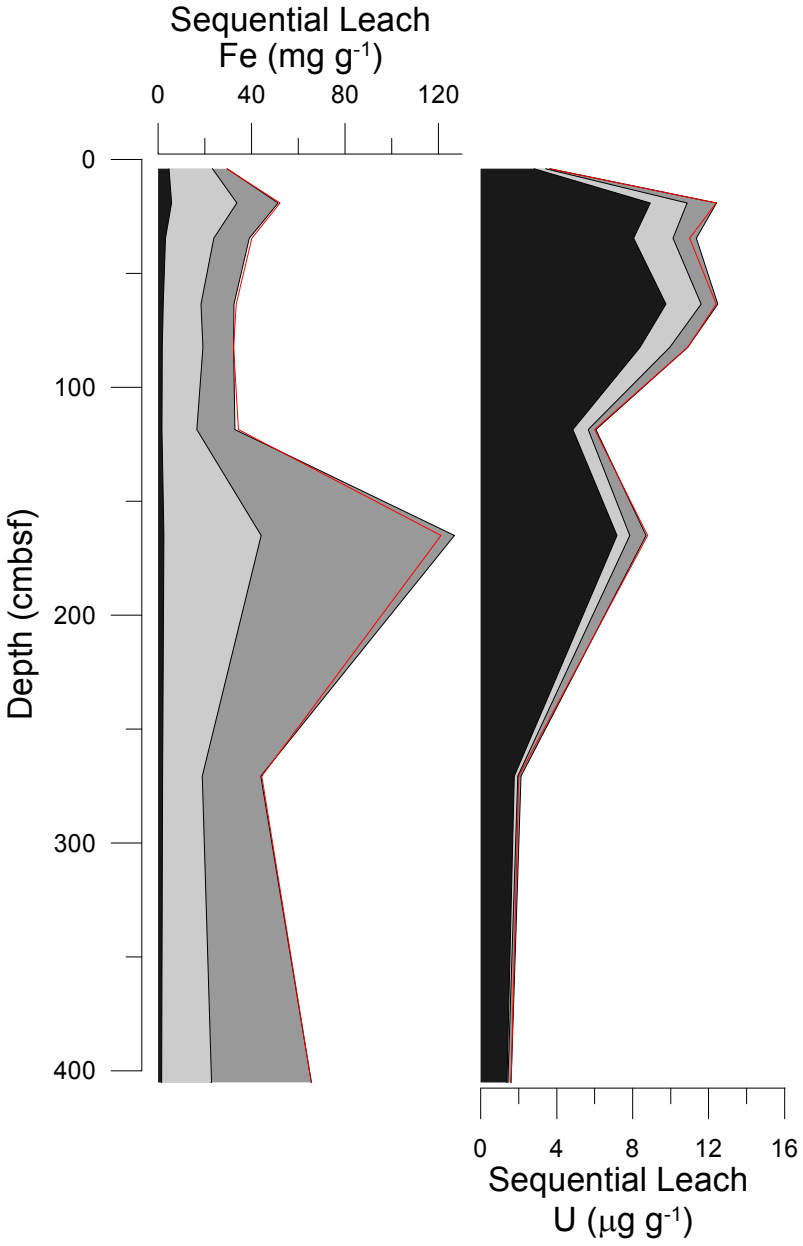
Sequential Leach
Fe (mg g-1)
0
40
80
120
0
100
200
300
400
Depth (cmbsf)
0
4
8
12
16
Sequential Leach
U (μg g-1)

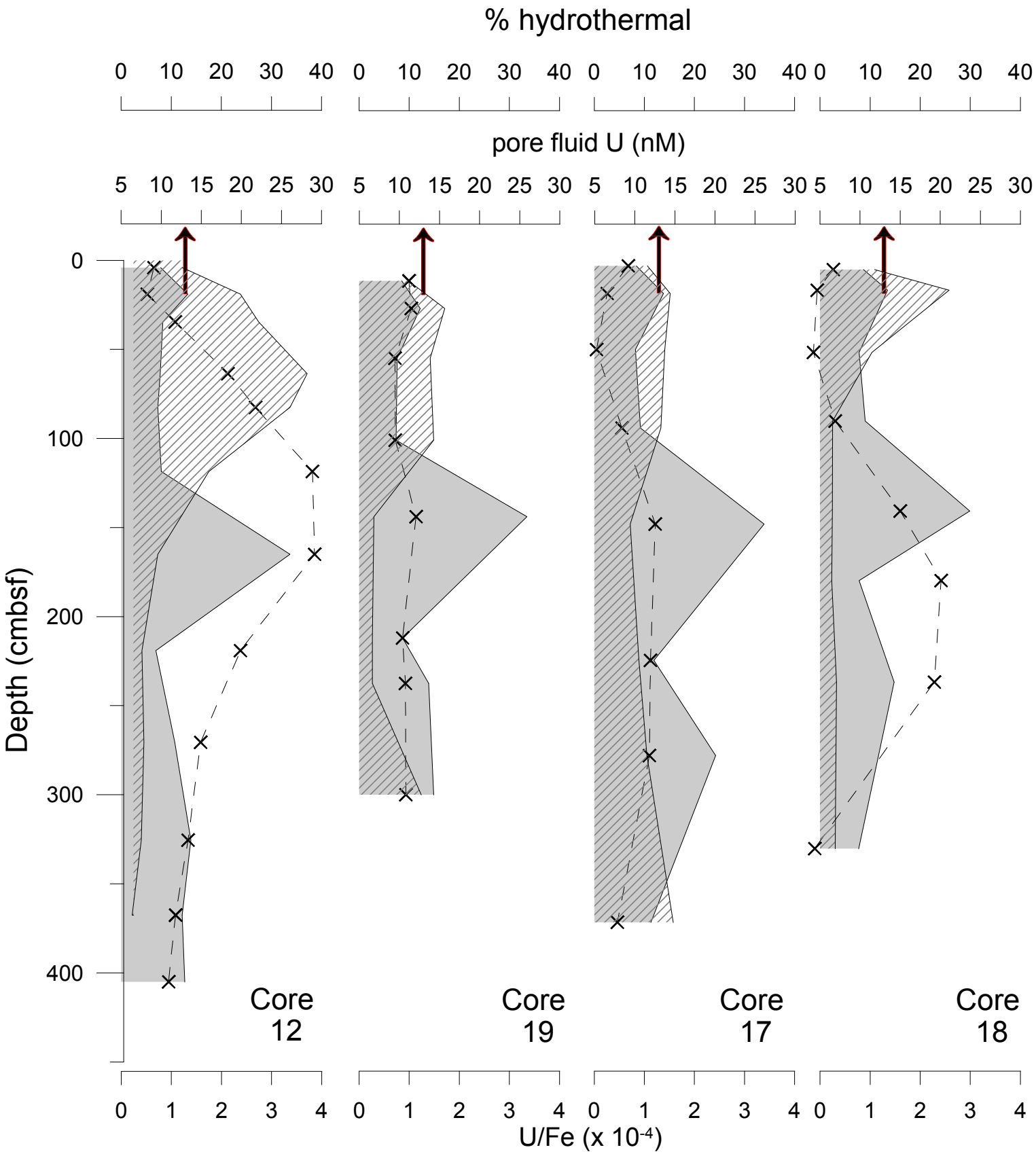
% hydrothermal
0 10 20 30 40
pore fluid U (nM)
5 10 15 20 25 30
Depth (cmbsf)
0
100
200
300
400
Core 12
Core 19
Core 17
Core 18
0 1 2 3 4
U/Fe (x 10-4)

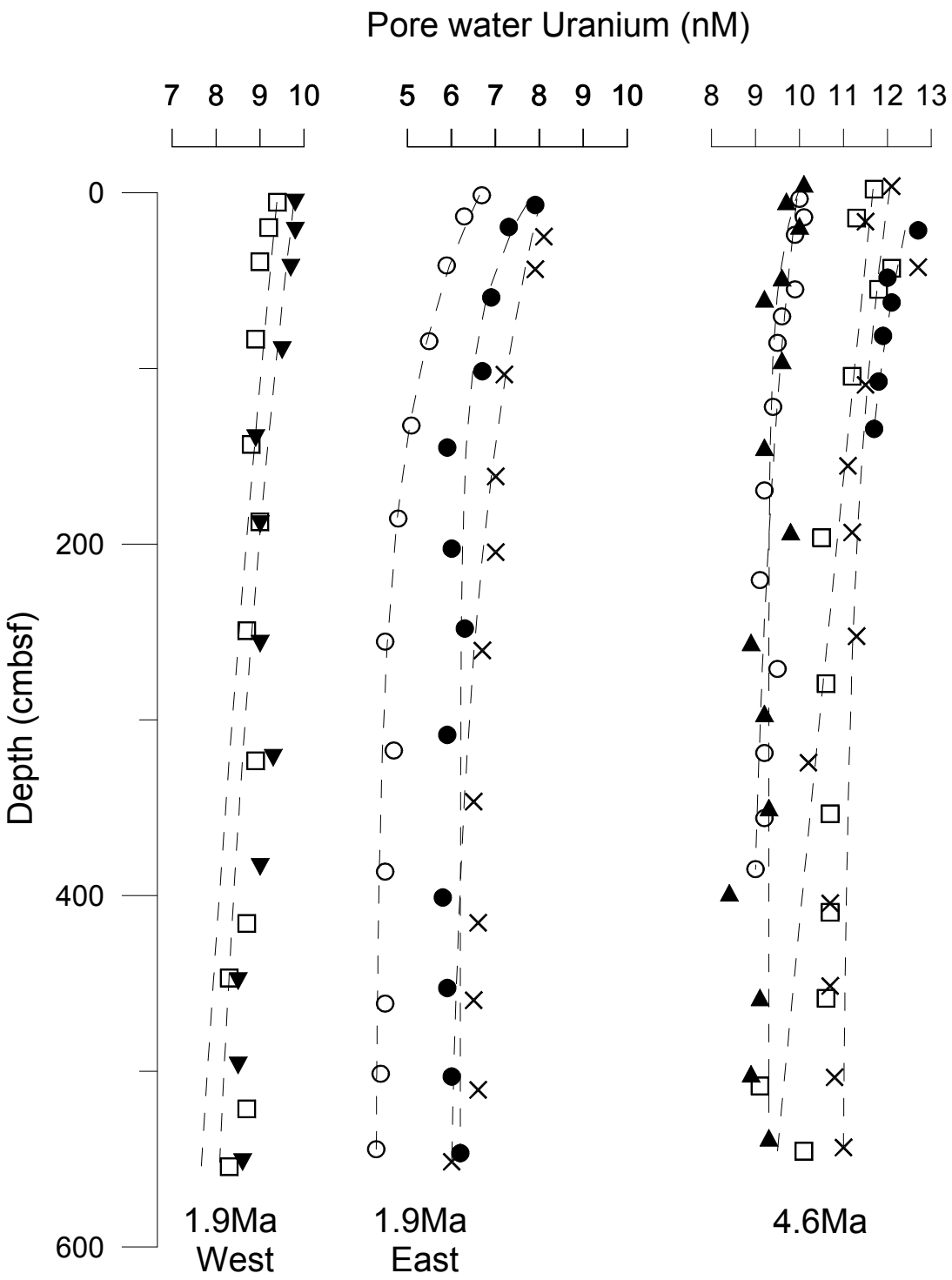
Pore water Uranium (nM)
7 8 9 10
5 6 7 8 9 10
8 9 10 11 12 13
0
200
400
600
Depth (cmbsf)
1.9Ma West
1.9Ma East
4.6Ma

Table 1: Core locations, basement U content and estimated upwelling velocity

Crustal Age	Core	Latitude	Longitude	Water Depth	Basement	upwelling	RMSD	[#]upwelling	RMSD
Ma		S	W	m	U nM	velocity mm yr^{-1}	nM	velocity mm yr^{-1}	mM
	11	14°16.82'	112°20.09'	3164		significant reaction			
	12	14°16.48'	112°19.38'	3047	10.9	significant reaction			
	13	14°16.72'	112°20.36'	3100		significant reaction			
0.36	14	14°16.94'	112°20.41'	3100		significant reaction			
	17	14°16.88'	112°19.84'	3089	15	significant reaction			
	18	14°16.73'	112°19.44'	3061		significant reaction		5.8	1.1
	19	14°16.54'	112°19.44'	3043	10.8	significant reaction			
	10	14°33.67'	111°15.2'	3190		7.5	0.25	4.3	0.72
	20	14°34.30'	111°17.1'	3239	8.3	0.3	0.45		
1.9	21	14°34.42'	111°16.56'	3209		0.7	0.34		
	23	14°34.66'	111°15.47'	3211		1.9	0.3	2.4	0.32
	24	14°33.75'	111°14.79'	3184	4.3	3.6	0.11	3.7	0.44
	4	14°55.86'	109°10.91'	3633		1.4	0.16		
	6	14°55.21'	109°10.32'	3486		significant reaction			
	7	14°58.29'	109°12.90'	3733		7.5	0.33		
4.6	25	14°56.61'	109°11.51'	3089		2	0.43		
	26	14°54.94'	109°10.73'	3061	11.7	2.4	0.15		
	27	14°56.24'	109°11.17'	3675		0.04	0.47		
	28	14°55.52'	109°10.65'	3583	11.3	no flow			
Seawater					13.9				

[#] = calculated from fluoride profiles (Mottl and Wheat, 2000)

Table 2: Sequential leach analysis of core 12

Iron

Depth m	CAE mg g^{-1}	AM mg g^{-1}	ORG mg g^{-1}	RES mg g^{-1}	Sum mg g^{-1}	Bulk Fe mg g^{-1}
0.04	4.7	18.5	0.13	6.28	29.6	29.5
0.19	5.7	28.0	0.04	17.7	51.4	52.2
0.35	3.1	20.6	0.12	15.2	39.0	40.1
0.64	2.3	16.0	0.05	14.1	32.5	33.4
0.83	1.8	17.3[#]	0.07	13.2	32.4	32.4
1.19	1.7	14.9	0.01	16.2	32.8	34.3
1.65	2.5	41.5	0.13	82.6	126.7	121
2.71	1.9	16.9	0.04	25.1	43.9	44.3
4.05	1.5	21.1[#]	0.16	42.8	65.6	65.6

Uranium

Depth m	CAE μg g^{-1}	AM μg g^{-1}	ORG μg g^{-1}	RES μg g^{-1}	Sum μg g^{-1}	Bulk U μg g^{-1}
0.04	2.81	0.61	0.08	0.16	3.7	3.6
0.19	8.94	1.93	0.06	1.49	12.4	12.4
0.35	8.06	2.06	0.22	1.02	11.4	11.0
0.64	9.76	1.84	0.09	0.79	12.5	12.4
0.83	8.39	1.57[#]	0.19	0.75	10.9	10.9
1.19	4.86	0.80	0.02	0.38	6.1	6.0
1.65	7.18	0.67	0.03	0.83	8.7	8.8
2.71	1.76	0.19	0.01	0.17	2.1	2.0
4.05	1.38	0.05[#]	0.02	0.15	1.6	1.6

[#] = leach not determined and therefore component estimated by difference

CAE = carbonate and adsorbed elements, AM = amorphous Fe oxides, ORG = organic phases and RES = residual

Sum = CAE + AM + ORG + RES